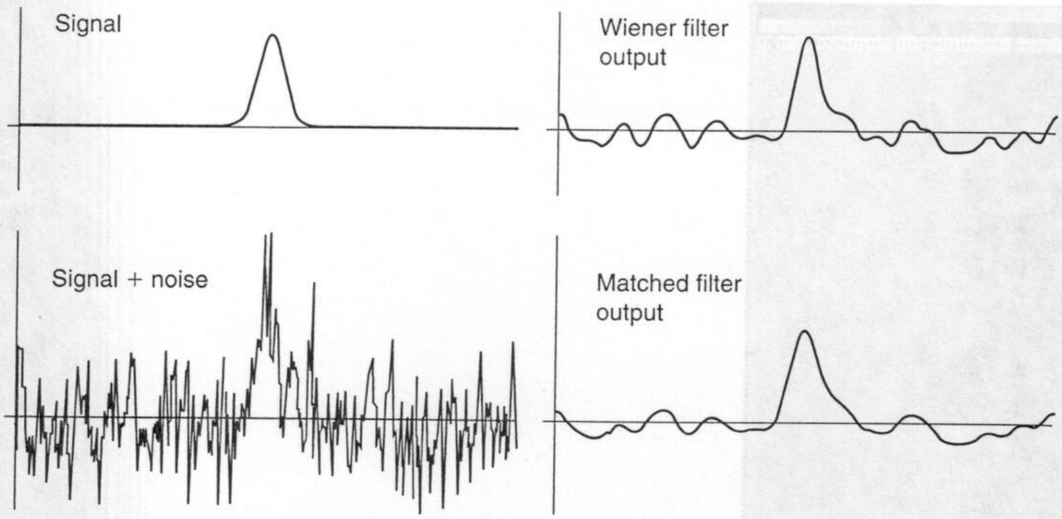

Figure 11–26 Comparison of the Wiener and matched filters

11.5.8 A Practical Example

We conclude the chapter with an example that illustrates how optimal filter theory can guide the design of practical filters. Figure 11–27 shows a digitized X ray of a tube filled with X-ray–absorbing dye. The image models angiography, a diagnostic technique in which dye is injected into blood vessels during X-ray exposure. Here, the smooth tube substitutes for the vessel.

The goal in this example is to develop a processing technique that will find the edges of the tube in the noisy image of Figure 11–27 and reliably measure the tube's diameter all along its length. Such a technique is useful for quantifying the narrowing of blood vessels that accompanies atherosclerosis and produces heart attacks [7].

Since the problem is one of edge detection, the matched detector would seem the natural choice. In this example, however, we pose the problem somewhat differently. We shall assume that the vessel's edges occur, on each image line, at the two points of steepest slope and attempt to locate these by differentiation. Before differentiating, however, we shall employ a Wiener filter to estimate the noise-free image. Furthermore, we shall process each horizontal scan line individually. This not only reduces the problem to a one-dimensional one, but also allows the procedure to respond to rapid changes in width, should they occur.

Figure 11–28 shows a gray-level plot of one line $f_i(x)$ from Figure 11–27. The evident noise is common in radiography, due primarily to film grain and photon statistics in the illuminating beam. Clearly, differentiating this curve would not produce reliable peaks at the inflection points, because of the noise.

Assuming uncorrelated signal $s(x)$ and noise $n(x)$, the specification of the Wiener filter [Eq. (59)] requires the power spectrum of the signal and that of the noise. We can estimate the signal's power spectrum by line averaging, since, with a smooth tube, all lines $f_i(x)$ should be identical in the absence of noise. Thus,

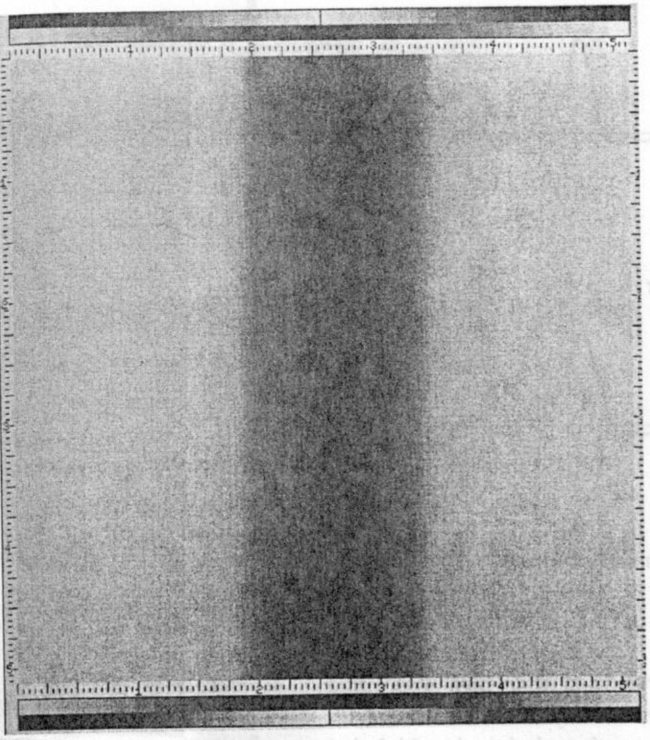

Figure 11–27 Digitized angiogram of a smooth tube

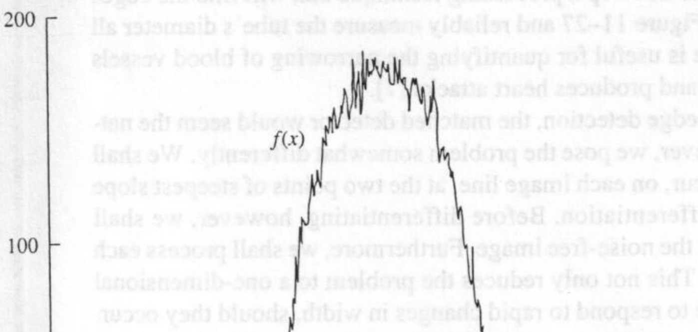

Figure 11–28 Line 100, Figure 11–27

$$P_s(s) = |\mathfrak{F}\{s(x)\}|^2 \approx \left|\mathfrak{F}\left\{\frac{1}{N}\sum_{i=1}^{N} f_i(x)\right\}\right|^2 \qquad (123)$$

will reduce the noise by the factor $1/\sqrt{N}$. Figure 11–29 shows the result of averaging 60 lines in Figure 11–27 and the resulting amplitude spectrum of the signal.

Once the signal has been estimated, the power spectrum of the noise can be estimated from Figure 11–27 using line-by-line power spectrum averaging after subtraction of the signal; that is,

$$P_n(s) \approx \frac{1}{N}\sum_{i=1}^{N} |\mathfrak{F}\{f_i(x) - s(x)\}|^2 \qquad (124)$$

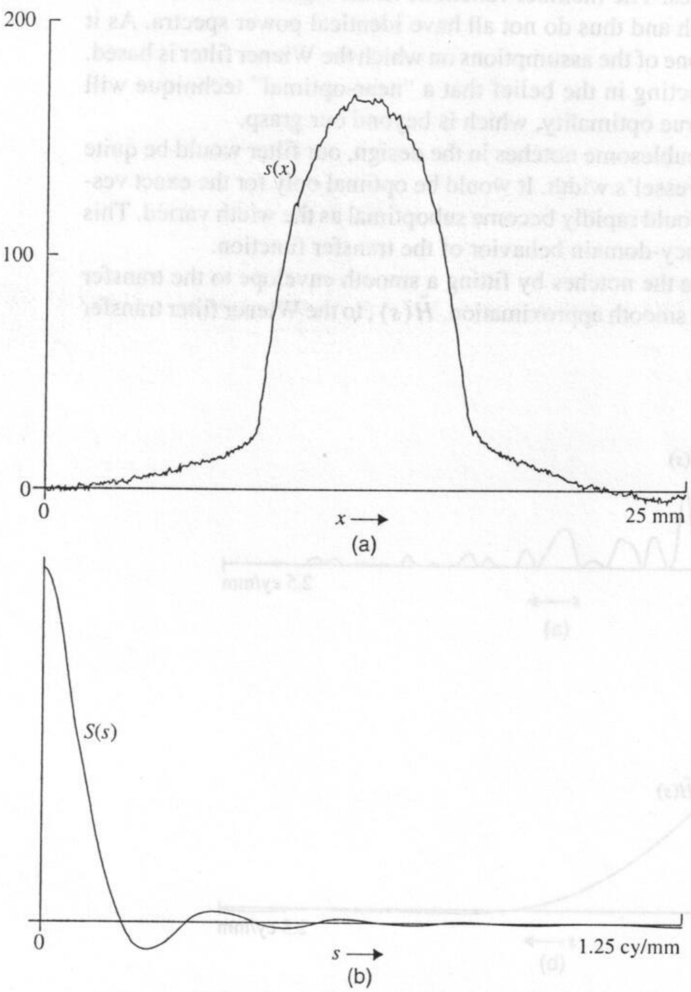

Figure 11–29 (a) Noise-free signal estimate obtained by line averaging in Figure 11–27; (b) Fourier amplitude spectrum of (a)

In this study, Eq. (124) showed the power spectrum of the noise to be essentially constant with frequency.

Figure 11–30(a) shows the Wiener filter transfer function $H_o(s)$ computed by Eq. (59). The transfer function takes on values near unity at the signal-dominated low frequencies and tends to zero at high frequencies.

We could inverse transform the transfer function in Figure 11–30(a) to obtain the impulse response for predifferentiation smoothing. There are, however, some practical considerations worthy of note.

The notches in the transfer function of Figure 11–30(a) are produced by the zero-crossings in the signal's spectrum [Figure 11–29(b)]. By the similarity theorem, the position of these notches will shift with changes in the width of the vessel.

This points up the fact that our signal is not actually an ergodic random process, as the Wiener filter development assumes. The member functions in the signal ensemble correspond to vessels of different width and thus do not all have identical power spectra. As it happens, we are forced to violate one of the assumptions on which the Wiener filter is based. We shall proceed nevertheless, acting in the belief that a "near-optimal" technique will prove an adequate substitute for true optimality, which is beyond our grasp.

If we were to include the troublesome notches in the design, our filter would be quite sensitive to slight changes in the vessel's width. It would be optimal only for the exact vessel width used in the design and would rapidly become suboptimal as the width varied. This is due to the rather abrupt frequency-domain behavior of the transfer function.

We choose instead to ignore the notches by fitting a smooth envelope to the transfer function. Figure 11–30(b) shows a smooth approximation, $\tilde{H}(s)$, to the Wiener filter transfer

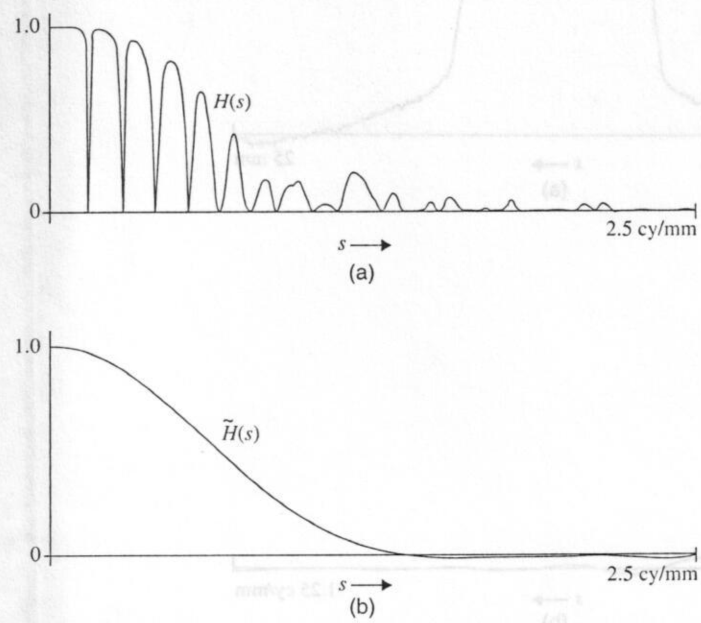

Figure 11–30 (a) Wiener filter transfer function; (b) smooth approximation to (a)

function. $\tilde{H}(s)$ was chosen because of two desirable properties: It is a reasonable approximation to the envelope of Figure 11–30(a), and its impulse response renders digital convolution quite an efficient computation.

Figure 11–31 shows the corresponding impulse response, $\tilde{h}(x)$, which is piecewise parabolic, and $\tilde{h}'(x)$, its first derivative, which is piecewise linear. Since differentiation commutes with convolution, using the latter function combines smoothing and differentiation into one step. Furthermore, digital convolution using a piecewise linear impulse response can be programmed to execute very efficiently [8].

Figure 11–32 shows the results of using the two impulse responses in Figure 11–31 on the image line in Figure 11–28. The first produces smoothing for noise reduction only, while the second combines smoothing with differentiation. In this case, the degree of noise reduction is gratifying. Notice also that the inflection points in the upper curve give rise to distinct peaks in the lower curve, suggesting that vessel edge detection is now a simple task.

The piecewise linear impulse response $\tilde{h}'(x)$ is a computationally efficient approximation to the differentiating Wiener filter for this application. Even though the signal is nonergodic, the notch-free transfer function $\tilde{H}(s)$ should be rather well behaved under suboptimal conditions, since it has no abrupt behavior in the frequency domain. Furthermore, Figure 11–32 strongly suggests that we have a comfortable solution to this edge detection

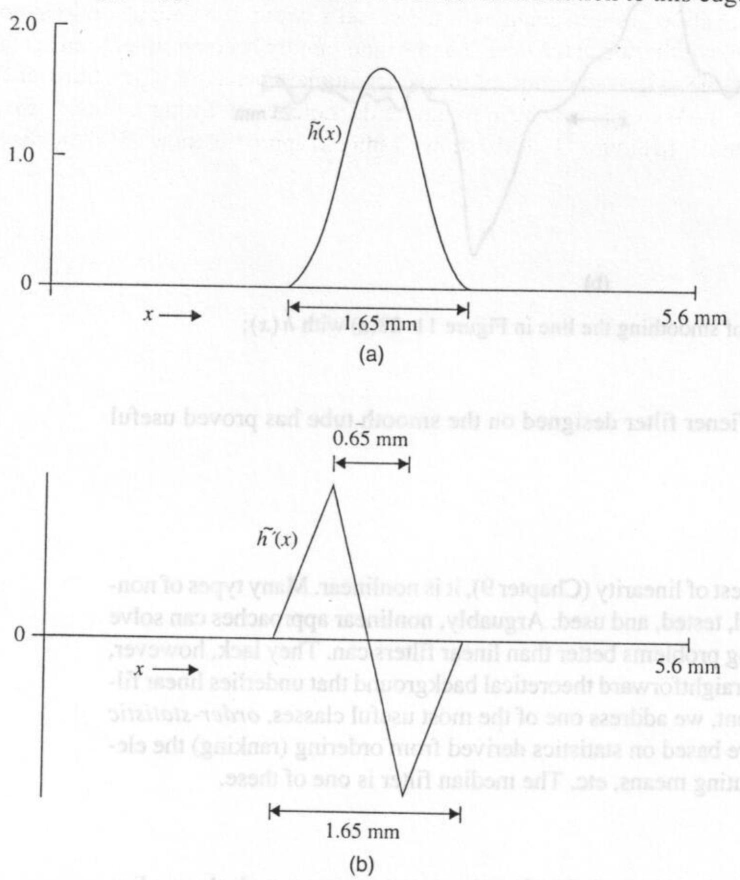

Figure 11–31 (a) Impulse response of Figure 11–30(b); (b) derivative of (a)

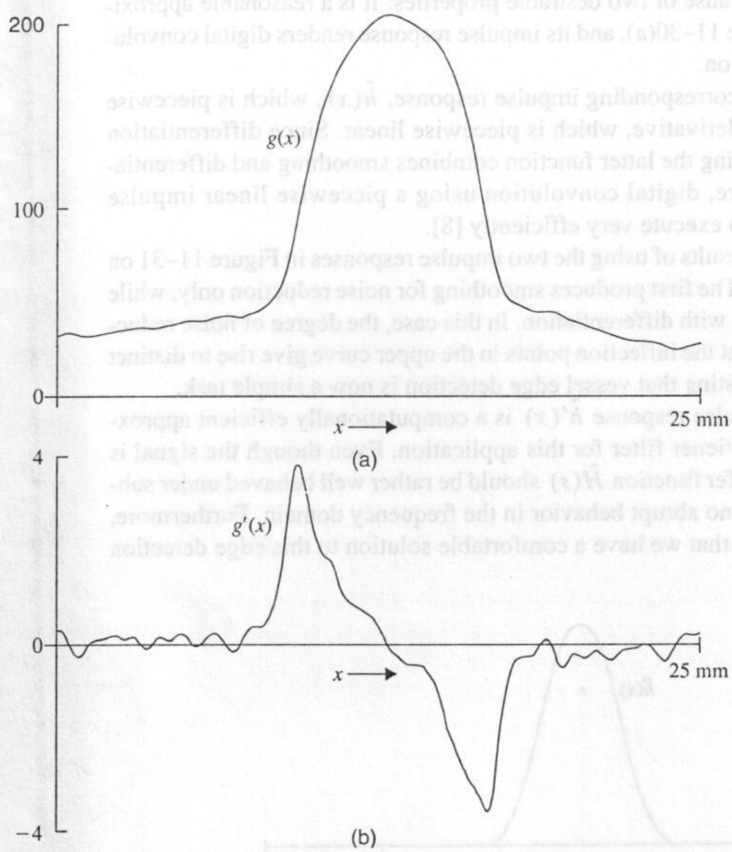

Figure 11–32 Results of smoothing the line in Figure 11–28(a) with $\bar{h}(x)$; (b) with $\bar{h}'(x)$

problem. The differentiating Wiener filter designed on the smooth tube has proved useful on routine angiograms [8].

11.6 ORDER-STATISTIC FILTERS

By definition, if a filter fails the test of linearity (Chapter 9), it is nonlinear. Many types of nonlinear filters have been described, tested, and used. Arguably, nonlinear approaches can solve certain types of image-processing problems better than linear filters can. They lack, however, the far-reaching and relatively straightforward theoretical background that underlies linear filters. For an introductory treatment, we address one of the most useful classes, *order-statistic filters,* so called because they are based on statistics derived from ordering (ranking) the elements of a set rather than computing means, etc. The median filter is one of these.

11.6.1 The Median Filter

The nonlinear filtering technique that has probably found most common usage is the median filter. It is a neighborhood operation, similar to convolution, except that the calculation is